

# Geomagnetic Signal of Millicharged Dark Matter

Ariel Arza,<sup>1,\*</sup> Yuanlin Gong,<sup>1,2,†</sup> Jing Shu,<sup>3,4,5,‡</sup> Lei Wu,<sup>1,§</sup> Qiang Yuan,<sup>2,6,¶</sup> and Bin Zhu<sup>7,\*\*</sup>

<sup>1</sup>*Department of Physics and Institute of Theoretical Physics,  
Nanjing Normal University, Nanjing, 210023, China*

<sup>2</sup>*Key Laboratory of Dark Matter and Space Astronomy,*

*Purple Mountain Observatory, Chinese Academy of Sciences, Nanjing 210023, China*

<sup>3</sup>*School of Physics and State Key Laboratory of Nuclear Physics and Technology, Peking University, Beijing 100871, China*

<sup>4</sup>*Center for High Energy Physics, Peking University, Beijing 100871, China*

<sup>5</sup>*Beijing Laser Acceleration Innovation Center, Huairou, Beijing, 101400, China*

<sup>6</sup>*School of Astronomy and Space Science, University of Science and Technology of China, Hefei 230026, China*

<sup>7</sup>*School of Physics, Yantai University, Yantai 264005, China*

Millicharge particles (mCPs) are viable dark matter candidates motivated by many standard model extensions. We show that despite of the tiny coupling with the photon, millicharged dark matters can convert efficiently to photons through annihilation processes in the Earth magnetic field background, which generates a monochromatic quasi static magnetic field signal with angular frequency being twice the millicharged particle mass. By recasting null results from the SuperMAG and the SNIPE Hunt collaborations, we constrain the effective charge of bosonic millicharged dark matter in the mass ranges  $10^{-18} - 3.5 \times 10^{-17}$  eV and  $10^{-15} - 10^{-14}$  eV. Our bounds surpass current stellar cooling constraints by more than ten orders of magnitude, making this proposal a powerful tool to search for millicharged dark matter.

**Introduction.** Identifying the nature of dark matter has been one of the frontiers in modern physics. Millicharged particles (mCPs), i.e., quantum fields with electric charges much smaller than the one  $e$  of the electron, are natural candidates [1–5]. mCPs can arise from models where the visible and a dark sectors are kinetically mixed [3, 6–10], or from models where these particles are directly charged under the  $U(1)_Y$  in the UV theory [11–13]. They are also widely predicted in string theory compactifications [11–16], and grand unification theories [17–19].

The masses of mCPs can span in a wide range. Depending on their masses, mCPs could have been produced in the early universe either via the freeze-in mechanism [20–23] or the misalignment mechanism [24–28]. In particular, the bosonic mCPs can be of a low mass (possibly even sub-eV) [29, 30], which might offer a solution to the small-scale structure problems and be relevant to astrophysical observations [31–33]. For example, mCPs with masses on the order of a few tens of MeV could account for the anomaly in the 21-cm signal if a small fraction of the dark matter is composed of them [34–38].

There have been various experiments and proposals capable to search for mCPs. They include cavities filled with strong electric field to probe Schwinger pair production [39–41], observation of the invisible decays of positronium [42], lamb shift of the hydrogen atom [43], laser polarization experiments [44–47], Cavendish experiment for testing Coulomb’s Law [48], timing of radio waves from pulsars and fast radio bursts [49], and direct deflection type experiments [50–52]. Meanwhile, astrophysical observations including the SN1987A [53, 54] and stellar evolution [55–59] have placed very strong constraints, and even more stringent ones can be obtained from galactic large scale magnetic fields [60] and cos-

mological measurements [30, 61], although the latter are highly model-dependent (for comprehensive reviews, see also [62, 63]).

In this work we propose a novel method to search for ultralight mCPs by detecting their induced magnetic signal on the Earth’s surface. In the Earth’s geomagnetic field background, a pair of mCPs can annihilate into a photon efficiently when the Compton wavelength of mCP field is bigger than the Earth size. Then a monochromatic quasi static magnetic field signal with angular frequency equal to twice the mCPs mass will be produced at any locations of the Earth’s surface. It is crucial to note that the effective current produced by the mCPs exhibits an inverse proportionality to the square of the mCP mass  $m_\phi$ , i.e.,  $J_\phi \sim 4e_m^2 B_0 R_e \rho / m_\phi^2$ , where  $e_m$  is the millicharge,  $B_0$  is the Earth’s geomagnetic field,  $R_e$  is the Earth’s radius, and  $\rho$  is the local dark matter energy density. This characteristic renders it extremely sensitive to ultra-light mCPs. In contrast, the effective current from dark photon dark matter  $J_{A'}$  is proportional to the dark photon mass  $m_{A'}$  as  $J_{A'} \sim \epsilon m_{A'} \sqrt{2\rho}$  [64, 65], where  $\epsilon$  is the kinetic mixing parameter. For axions, the corresponding effective current  $J_a$  shows no dependence on the axion mass  $m_a$  as  $J_a \sim g_{a\gamma} B_0 \sqrt{2\rho}$  [66], where  $g_{a\gamma}$  is the coupling of axion with two photons.

By reinterpreting null results for axion and dark photon searches from the SuperMAG [64–66] and SNIPE Hunt [67] collaborations, we estimate a world-leading bound on ultralight mCPs dark matter, which surpasses the existing constraints from stellar cooling by more than ten orders of magnitude. Consequently, it is expected that future dedicated measurements of the magnetic activity on the Earth’s surface will open up new avenues for the exploration of mCPs on different mass ranges and smaller values of  $e_m$ .

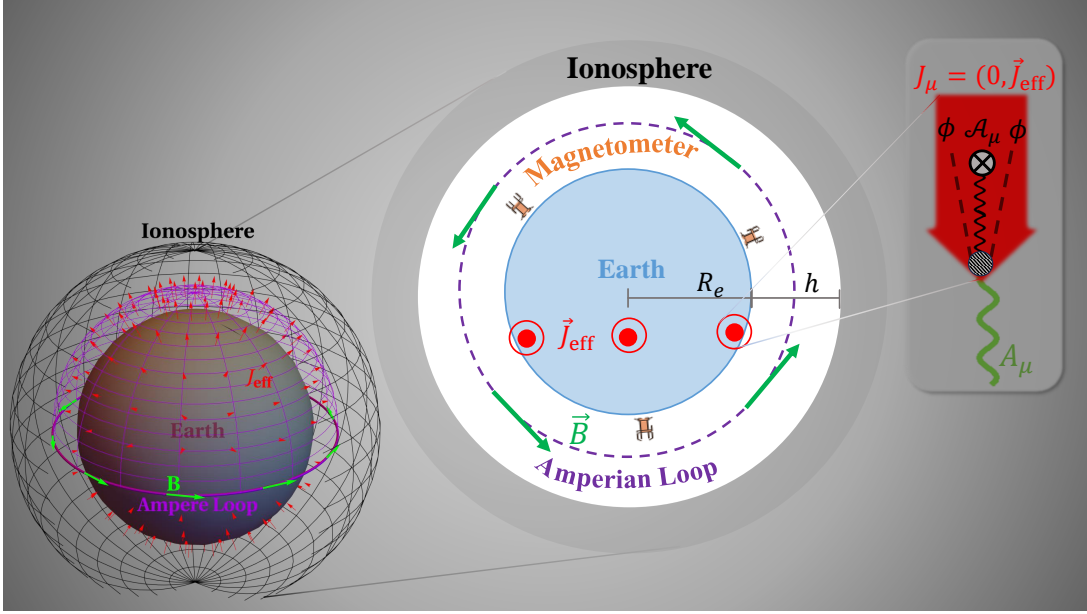


Figure 1. **Middle:** Natural Earth's cavity formed between the Earth's surface and the ionosphere. It shows the radial component of the dark matter effective current  $\vec{J}_{\text{eff}}$  passing through a chosen Amperian Loop. The generated magnetic field  $\vec{B}$  can be probed by the magnetometers (orange symbols) placed over the surface of the Earth. **Lower Left:** It shows the 3D version of the Middle, in where the effective current is depicted from Eq. (7). **Upper Right:** It shows the annihilation of two millicharged particles in the external magnetic field background.

***mCP Electrodynamics.*** The interaction between the ultralight bosonic mCP field  $\phi$  and the photon field  $A_\mu$  is described by the following lagrangian

$$\mathcal{L} = D_\mu \phi (D^\mu \phi)^* - m_\phi^2 |\phi|^2 - \frac{1}{4} F_{\mu\nu} F^{\mu\nu}, \quad (1)$$

where  $D_\mu = \partial_\mu + ie_m A_\mu$  is the covariant derivative and  $F_{\mu\nu} = \partial_\mu A_\nu - \partial_\nu A_\mu$  is the electromagnetic strength tensor. Since the occupancy number for mCP with mass below the eV is quite high, we can treat the mCP field as a classical wave, and derive the induced electromagnetic signal from the modified Maxwell's equations.

For a given external electromagnetic field  $\mathcal{A}_\mu = (\mathcal{A}_0, -\vec{\mathcal{A}})$ , after neglecting small nonlinear terms, the equations of motion (EoMs) are then written as

$$\begin{aligned} \partial_\mu F^{\mu\nu} &= J_m^\nu - 2e_m^2 \mathcal{A}^\nu |\phi|^2 \equiv J_{\text{eff}}^\nu, & (2) \\ (\square + m_\phi^2)\phi &= -ie_m \partial_\mu \mathcal{A}^\mu \phi - 2ie_m \partial_\mu \phi \mathcal{A}^\mu \\ &\quad + e_m^2 \mathcal{A}_\mu \mathcal{A}^\mu \phi. & (3) \end{aligned}$$

where  $J_m^\nu = ie_m (\phi^* \partial^\nu \phi - \phi \partial^\nu \phi^*)$  is the millicharged current. Due to the very small coupling  $e_m$ , we can adopt perturbation theory to find the solutions to Eqs. (2) and (3). These EoMs are gauge invariant under the transformation  $\mathcal{A}'_\mu = \mathcal{A}_\mu + \partial_\mu \Lambda$  and  $\phi' = \phi e^{-ie_m \Lambda}$ , where  $\Lambda$  is the arbitrary gauge function. We choose Coulomb gauge,  $\vec{\nabla} \cdot \vec{\mathcal{A}} = 0$  and  $\mathcal{A}_0 = 0$ , and expand the millicharged field to first order in  $e_m$  as  $\phi = \phi_0 + \phi_1$ , where the zeroth-

order term is the charge symmetric millicharged field background given by  $\phi_0 = \frac{\sqrt{2\rho}}{m_\phi} \cos(\vec{k}_\phi \cdot \vec{x} - m_\phi t)$ , with  $k_\phi$  being the momentum of the mCPs<sup>1</sup>. The background field satisfies  $(\square + m_\phi^2)\phi_0 = 0$  while the first-order term  $\phi_1$  is determined by the differential equation  $(\square + m_\phi^2)\phi_1 = -2ie_m \vec{\nabla} \phi_0 \cdot \vec{\mathcal{A}}$  under the boundary condition  $\phi_1 = 0$  for  $|\vec{x}| \rightarrow \infty$ . Once  $\phi_1$  is known, we can reduce Eq. (2) to

$$\square \vec{\mathcal{A}} = 2e_m \phi_0 \text{Im}(\vec{\nabla} \phi_1) - 2e_m^2 \vec{\mathcal{A}} \phi_0^2. \quad (4)$$

The first term of the right-hand side of the above equation is suppressed by the mCP velocity,  $v \sim 10^{-3}$ , because of the gradient operator. The second term is the effective current that gives us the main contribution for the signal. This effective current features a  $1/m_\phi^2$  dependence, which as mentioned in the introduction, is quite different from the cases of axion and dark photon dark matter [64–66], and provides an opportunity to search for the millicharged dark matter in very low mass range.

***Experimental setup and Sensitivity.*** Let us consider a region of size  $L$  that is bounded by a conducting shielding. A dark matter induced oscillating effective current  $J_{\text{eff}}$  drives an electromagnetic field inside the region

<sup>1</sup> To satisfy charge symmetry, the field may also be multiplied by the factor  $e^{i\chi}$ , where  $\chi$  is an arbitrary constant phase. However, this constant phase is not physical and does not intervene in neither the calculations nor the results, therefore we just choose it equal to zero.

that is damped in the boundaries. When the frequency of the oscillating current is much smaller than  $1/L$ , the signal is dominated by a quasi static magnetic field whose strength is roughly of the form  $B \sim J_{\text{eff}}L$ . Based on this, novel experimental ideas for axions [68, 69] and also dark photons [70] were proposed at the laboratory scale for masses between  $10^{-10}$  and  $10^{-6}$  eV, where one can benefit from resonant signal enhancements and strict control of the background noise.

In this work, we propose to search for bosonic millicharged dark matter by applying the same principle mentioned above to the huge natural Earth conducting cavity. As illustrated in Fig. 1, the Earth can play a role of a natural cavity, shielded from below by the Earth's surface and from above by the ionosphere (or interplanetary medium). We set the Earth's radius as  $R_e = 6371.2$  km, therefore the proposal applies for masses below  $1/R_e \sim 10^{-14}$  eV. For such low masses, we benefit in sensitivity due to the Earth size and the  $1/m_\phi^2$  scaling of the signal, then using high precision magnetometers situated over the surface of the Earth, it is possible to probe ultralight mCPs dark matter in a wide unexplored parameter space.

The profile of the vector potential  $\vec{\mathcal{A}}$  above the Earth's surface is determined by the profile of the geomagnetic field  $\vec{\mathcal{B}}$  extended over the whole Earth's region. We use the updated IGRF model [71] to describe the geomagnetic field from the atmosphere into the mantle, while for the inner and outer core, we model it by resorting to the electric current that produces it. The most popular theory about the origin of the Earth's magnetic field is the geodynamo, in which the geomagnetic field is generated by electric currents  $\vec{J}$  in the Earth's outer core [72, 73]. Currents in the solid inner core and the mantle are vanishing. To get the profile of  $\vec{J}$ , we use polynomial functions that fit the rms value of the geomagnetic field  $\mathcal{B}$  over the outer core and respect appropriate boundary conditions. Then, the magnetic field  $\vec{\mathcal{B}}$  and vector potential  $\vec{\mathcal{A}}$  can be calculated by solving  $\nabla \times \vec{\mathcal{B}} = \vec{J}$  and  $\nabla \times \vec{\mathcal{A}} = \vec{\mathcal{B}}$ , respectively, together with the conditions  $\vec{\nabla} \cdot \vec{\mathcal{B}} = 0$  and  $\vec{\nabla} \cdot \vec{\mathcal{A}} = 0$ . See all the details of this calculation in Supplementary Material.

As a result, the external vector potential above the Earth's surface, i.e.,  $r \geq R_e$ , is given by

$$\vec{\mathcal{A}} = -B_0 R_e \left( 1.01\beta \left( \frac{R_e}{r} \right)^3 (2\vec{Y}_{10} - \vec{\Psi}_{10}) - \sqrt{\frac{4\pi}{3}} \left( \frac{R_e}{r} \right)^2 \vec{\Phi}_{10} \right), \quad (5)$$

where  $B_0 = 2.94 \times 10^{-2}$  mT is the total geomagnetic field at the equator of the Earth's surface and  $\vec{Y}_{10}$ ,  $\vec{\Psi}_{10}$ ,  $\vec{\Phi}_{10}$  are vector spherical harmonics (VSH). The parameter  $\beta$  accounts for the uncertainty in the rms value of the geomagnetic field  $\mathcal{B}$  in the outer core. The value of  $\beta$  ranges

between 1 and 4.6.

Knowing the external vector potential  $\vec{\mathcal{A}}$ , we can analytically solve Eq. (4). For our mass range of interest, where  $m_\phi \ll 1/R_e$  is satisfied, Eq. (4) can be approximated to the magneto quasi static equation

$$\vec{\nabla} \times \vec{\mathcal{B}} = \vec{J}_{\text{eff}}, \quad (6)$$

where  $\vec{\mathcal{B}} = \vec{\nabla} \times \vec{\mathcal{A}}$  is the magnetic field signal and  $\vec{J}_{\text{eff}}$  the dark matter effective current given by

$$\vec{J}_{\text{eff}} = \frac{2e_m^2 \rho B_0 R_e}{m_\phi^2} \left( 1.01\beta \left( \frac{R_e}{r} \right)^3 (2\vec{Y}_{10} - \vec{\Psi}_{10}) - \sqrt{\frac{4\pi}{3}} \left( \frac{R_e}{r} \right)^2 \vec{\Phi}_{10} \right) e^{-2im_\phi t}. \quad (7)$$

In our calculation, we use the fact that both the Earth surface and the ionosphere layers are well conductors. Then, Eq. (6) can be solved with the boundary condition  $\vec{B}_r = 0$  at  $r = R_e$  and  $r = R_e + h$ , where  $\vec{B}_r$  is the radial component of the magnetic field and  $h$  is the ionosphere height. We note that, at very low frequencies and depending on solar activity and other factors, the ionosphere may not be a good conductor that can damp the electromagnetic active mode completely. In such a case the upper boundary would be the interplanetary medium. For more details of the ionosphere and interplanetary medium conducting properties, see Ref. [64].

Finally, by solving Eq. (6) together with the condition  $\vec{\nabla} \cdot \vec{\mathcal{B}} = 0$ , the magnetic field signal at the Earth's surface is given by

$$\vec{\mathcal{B}}(t) = \frac{e_m^2 \rho B_0 R_e^2}{m_\phi^2} \left( \sqrt{\frac{4\pi}{3}} \frac{h}{R_e} \vec{\Psi}_{10} - 2.02\beta \vec{\Phi}_{10} \right) e^{-i2m_\phi t}. \quad (8)$$

The dominant contribution comes from the  $\vec{\Phi}_{10}$  term of the signal. The suppression factor  $h/R_e \ll 1$  in the  $\vec{\Psi}_{10}$  term can be understood from the Ampere's law  $\oint d\vec{l} \cdot \vec{\mathcal{B}} = \int d\vec{S} \cdot \vec{J}_{\text{eff}}$ , where an integral loop is shown in Fig. S2 in the Supplementary Material. For pure tangential components of the effective current in Eq. (7), i.e. the  $\vec{\Phi}_{10}$  term, the integral  $\int d\vec{S} \cdot \vec{J}_{\text{eff}}$  gives  $\sim \pi R_e h J_{\text{eff}}$ , while  $\oint d\vec{l} \cdot \vec{\mathcal{B}}$  becomes  $\sim B R_e$ , resulting in  $|B| \sim \pi R_e (h/R_e) J_{\text{eff}}$ . On the other hand, for radial components of the effective current, such as the  $\vec{Y}_{10}$  term in Eq. (7), we can use the amperian loop shown in Fig. 1 to obtain  $\int d\vec{S} \cdot \vec{J}_{\text{eff}} \sim \pi R_e^2 J_{\text{eff}}$ , leading to  $B \sim \pi R_e J_{\text{eff}}$ .

For  $R_e = 6371.2$  km,  $B_0 = 2.94 \times 10^{-2}$  T,  $\beta = 1$  and  $\rho = 0.3$  GeV/cm<sup>3</sup>, we notice that the amplitude of the

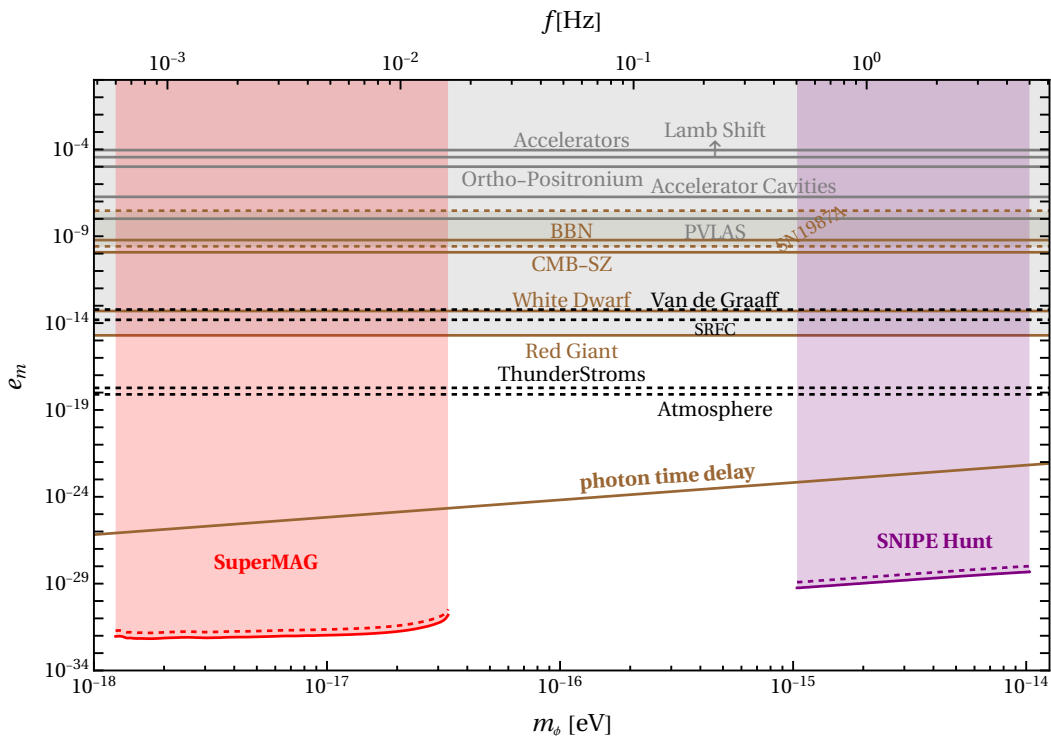


Figure 2. Projected sensitivity on millicharged dark matter in the  $(m_\phi, e_m)$  space of parameters. The red and purple shaded regions are roughly exclusions by reinterpreting the null results of searching for axion from the SuperMAG and SNIPE Hunt collaborations. The dashed (solid) lines correspond to  $\beta = 1$  (4.6) reflecting the uncertainty on the geomagnetic field rms value over the Earth’s outer core. We also plot experimental constraints from accelerators [58], Lamb shift [43], Ortho-Positronium [42], accelerator cavities [44] and PVLAS experiment [47]. Previous astrophysical and cosmological observation bounds (brown solid lines) including CMB observations of the Sunyaev-Zel’dovich effect [74], SN1987A [54], red giants [58], white dwarfs [58] and BBN [75] are also shown. The dashed black lines are projected sensitivities from superconducting radio-frequency cavities [40] and millicharged condensates [76]. Additionally, a constraint from photon time delay of pulsars induced by the mCP is included (See Supplemental Material for a derivation of this constraint).

magnetic field signal is

$$|B| = 696 \text{ pT} \left( \frac{e_m}{10^{-27}} \right)^2 \left( \frac{10^{-14} \text{ eV}}{m_\phi} \right)^2, \quad (9)$$

meaning that for our mass ranges of interest, which correspond to signal frequencies below 5 Hz, a mCP field can produce a magnetic field signal of hundreds of pT for millicharges down to  $e_m = 10^{-27}$ . Current unshielded magnetometers can easily reach this sensitivities. To have an idea, in the first campaign of the SNIPE Hunt collaboration, magnetometers with  $300 \text{ pT}/\sqrt{\text{Hz}}$  were used [67].

A straightforward concern for a dedicated experimental exploration are the background noises. For the frequencies that interests us, the dominant magnetic field sources are anthropogenic [77], so to get optimal sensitivity, the experiment can be set up in a remote location, far from urban environments. Moreover, the dark matter signal oscillates at a particular frequency that makes it easy to be distinguished from static sources, such as the strong static Earth’s geomagnetic field. In fact, it

was demonstrated in the first SNIPE Hunt expedition, that the amplitude spectral density of the measurements were flat and corresponded to the noise floor of the magnetometers, with the exception of a 60 Hz peak associated with the laptop used for data acquisition. While a few narrow peaks at one of the measurement stations are attributed to noise with unknown origin since the dark matter signal should be present in all stations at all times. In addition, since the reach of the SNIPE Hunt is now limited by the sensitivity of the magnetometers [67], rather than by the geomagnetic noise, future dedicated experiments using high-precision magnetometers with sensitivity up to order  $20 \text{ fT}/\sqrt{\text{Hz}}$  [78–81] will result in stronger sensitivity.

In Fig. 2, we show constraints for dark matter mCPs by recasting the null results of searching for axion and dark photon from the SuperMAG [64–66] and SNIPE Hunt [67] collaborations. The SNIPE Hunt collaboration performed coordinated measurements with a network of magnetometers located in the US, in three different stations far from human-generated magnetic noise. Each station used a vector magnetoresistive sensor with

sensitivity of  $300 \text{ pT}/\sqrt{\text{Hz}}$  over a frequency range of  $0.1 - 100 \text{ Hz}$  [67] to measure the signal. The SuperMAG data consist of measurements taken with a one-minute cadence across several tens of years, with contributions from  $\mathcal{O}(500)$  stations all over the world [64–66]. To obtain the SNIPE Hunt constraints for dark matter mCPs, we first calculate the magnetic field amplitude  $|\vec{B}_a|$  by using the constraints found in Ref. [67] for three different stations and then we obtain an averaged value. In the same frequency, we equal this average to the counterpart magnetic field signal in Eq. (8) to estimate the bounds on  $e_m$ . For the SuperMAG constraints, since the data are collected with many stations situated over the world, we instead average the  $\vec{B}_a$  over the Earth’s surface to get magnetic field expressions independent on the Earth location. Then we proceed in the same way as done for SNIPE Hunt. As we can see in Fig. 2, the estimated constraints surpass previous bounds from stellar cooling by over ten orders of magnitude in the case of SNIPE Hunt and over seventeen orders of magnitude for SuperMAG, which could be further improved by using more high precision magnetometers [78–81].

**Conclusion.** We have presented a novel approach to probe the ultralight millicharged dark matters (mCPs) by measuring their geomagnetic signals. Using classical field theory we calculated the quasi static monochromatic magnetic field signal sourced by the effective current associated with the millicharged dark matter field, which shows a unique inverse proportionality to the square of the mCPs mass. By reinterpreting the data from the SuperMAG and SNIPE Hunt experiments, we have estimated stringent constraints on the effective charge of dark matter bosonic mCPs in specific mass ranges. These constraints are up to seventeen orders of magnitude stronger than stellar cooling bounds. Finally, the search for mCPs as a dark matter, by monitoring the Earth’s magnetic activity utilizing high-precision magnetometers, holds great potential for further advancements in this field. Future dedicated measurements of the Earth’s magnetic activity are expected to yield even stronger sensitivity and the possibility to explore dark matter mCPs in other mass ranges, facilitating a deeper understanding of the nature of dark matter.

**Acknowledgement.** We would like to thank Itay Bloch and Saarik Kalia for useful discussions and also Yuxin Liu for the insight and discussion on the constraint from the photon time delay of pulsars. L.W. is supported by the National Natural Science Foundation of China (NSFC) under Grants No. 12275134, No. 12335005, and No. 12147228. J.S. is supported by the National Key Research and Development Program of China under Grants No. 2020YFC2201501 and No. 2021YFC2203004, Peking University under startup Grant No. 7101302974, the NSFC under Grants No. 12025507, No. 12150015, No. 12450006, and the Key Research Program of Frontier Science of the Chinese

Academy of Sciences (CAS) under Grant No. ZDBS-LY-7003. Q.Y. is supported by the NSFC under Grant No. 12220101003 and the Project for Young Scientists in Basic Research of the CAS under Grant No. YSBR-061. B.Z. is supported by the NSFC under Grant No. 12275232.

---

\* ariel.arza@gmail.com

† yuanlingong@nnu.edu.cn

‡ jshu@pku.edu.cn

§ leiwu@njnu.edu.cn

¶ yuanq@pmo.ac.cn

\*\* zhubin@mail.nankai.edu.cn

- [1] S. Dimopoulos, D. Eichler, R. Esmailzadeh, and G. D. Starkman, *Phys. Rev. D* **41**, 2388 (1990).
- [2] A. De Rujula, S. L. Glashow, and U. Sarid, *Nucl. Phys. B* **333**, 173 (1990).
- [3] D. Feldman, Z. Liu, and P. Nath, *Phys. Rev. D* **75**, 115001 (2007), [arXiv:hep-ph/0702123](#).
- [4] S. D. McDermott, H.-B. Yu, and K. M. Zurek, *Phys. Rev. D* **83**, 063509 (2011), [arXiv:1011.2907 \[hep-ph\]](#).
- [5] J. M. Cline, Z. Liu, and W. Xue, *Phys. Rev. D* **85**, 101302 (2012), [arXiv:1201.4858 \[hep-ph\]](#).
- [6] B. Holdom, *Phys. Lett. B* **166**, 196 (1986).
- [7] H. Goldberg and L. J. Hall, *Phys. Lett. B* **174**, 151 (1986).
- [8] E. Izaguirre and I. Yavin, *Phys. Rev. D* **92**, 035014 (2015), [arXiv:1506.04760 \[hep-ph\]](#).
- [9] K. Cheung and T.-C. Yuan, *JHEP* **03**, 120 (2007), [arXiv:hep-ph/0701107](#).
- [10] W.-Z. Feng, Z.-H. Zhang, and K.-Y. Zhang, *JCAP* **05**, 112 (2024), [arXiv:2312.03837 \[hep-ph\]](#).
- [11] X.-G. Wen and E. Witten, *Nucl. Phys. B* **261**, 651 (1985).
- [12] G. Shiu, P. Soler, and F. Ye, *Phys. Rev. Lett.* **110**, 241304 (2013), [arXiv:1302.5471 \[hep-th\]](#).
- [13] W.-Z. Feng, G. Shiu, P. Soler, and F. Ye, *Phys. Rev. Lett.* **113**, 061802 (2014), [arXiv:1401.5880 \[hep-ph\]](#).
- [14] C. P. Burgess, J. P. Conlon, L.-Y. Hung, C. H. Kom, A. Maharana, and F. Quevedo, *JHEP* **07**, 073 (2008), [arXiv:0805.4037 \[hep-th\]](#).
- [15] M. Goodsell, J. Jaeckel, J. Redondo, and A. Ringwald, *JHEP* **11**, 027 (2009), [arXiv:0909.0515 \[hep-ph\]](#).
- [16] M. Cicoli, M. Goodsell, J. Jaeckel, and A. Ringwald, *JHEP* **07**, 114 (2011), [arXiv:1103.3705 \[hep-th\]](#).
- [17] J. C. Pati and A. Salam, *Phys. Rev. D* **8**, 1240 (1973).
- [18] H. Georgi, *AIP Conf. Proc.* **23**, 575 (1975).
- [19] J. Preskill, *Ann. Rev. Nucl. Part. Sci.* **34**, 461 (1984).
- [20] L. J. Hall, K. Jedamzik, J. March-Russell, and S. M. West, *JHEP* **03**, 080 (2010), [arXiv:0911.1120 \[hep-ph\]](#).
- [21] R. Essig, J. Mardon, and T. Volansky, *Phys. Rev. D* **85**, 076007 (2012), [arXiv:1108.5383 \[hep-ph\]](#).
- [22] X. Chu, T. Hambye, and M. H. G. Tytgat, *JCAP* **05**, 034 (2012), [arXiv:1112.0493 \[hep-ph\]](#).
- [23] C. Dvorkin, T. Lin, and K. Schutz, *Phys. Rev. D* **99**, 115009 (2019), [Erratum: *Phys. Rev. D* 105, 119901 (2022)], [arXiv:1902.08623 \[hep-ph\]](#).
- [24] J. Preskill, M. B. Wise, and F. Wilczek, *Phys. Lett. B* **120**, 127 (1983).
- [25] L. F. Abbott and P. Sikivie, *Phys. Lett. B* **120**, 133 (1983).

- [26] M. Dine and W. Fischler, *Phys. Lett. B* **120**, 137 (1983).
- [27] A. E. Nelson and J. Scholtz, *Phys. Rev. D* **84**, 103501 (2011), [arXiv:1105.2812 \[hep-ph\]](#).
- [28] P. Arias, D. Cadamuro, M. Goodsell, J. Jaeckel, J. Redondo, and A. Ringwald, *JCAP* **06**, 013 (2012), [arXiv:1201.5902 \[hep-ph\]](#).
- [29] G. Alonso-Álvarez, J. Gehrlein, J. Jaeckel, and S. Schenk, *JCAP* **09**, 003 (2019), [arXiv:1906.00969 \[hep-ph\]](#).
- [30] J. Jaeckel and S. Schenk, *Phys. Rev. D* **103**, 103523 (2021), [arXiv:2102.08394 \[hep-ph\]](#).
- [31] W. Hu, R. Barkana, and A. Gruzinov, *Phys. Rev. Lett.* **85**, 1158 (2000), [arXiv:astro-ph/0003365](#).
- [32] L. Hui, J. P. Ostriker, S. Tremaine, and E. Witten, *Phys. Rev. D* **95**, 043541 (2017), [arXiv:1610.08297 \[astro-ph.CO\]](#).
- [33] E. G. M. Ferreira, *Astron. Astrophys. Rev.* **29**, 7 (2021), [arXiv:2005.03254 \[astro-ph.CO\]](#).
- [34] J. B. Muñoz and A. Loeb, *Nature* **557**, 684 (2018), [arXiv:1802.10094 \[astro-ph.CO\]](#).
- [35] A. Berlin, D. Hooper, G. Krnjaic, and S. D. McDermott, *Phys. Rev. Lett.* **121**, 011102 (2018), [arXiv:1803.02804 \[hep-ph\]](#).
- [36] T. R. Slatyer and C.-L. Wu, *Phys. Rev. D* **98**, 023013 (2018), [arXiv:1803.09734 \[astro-ph.CO\]](#).
- [37] E. D. Kovetz, V. Poulin, V. Gluscevic, K. K. Boddy, R. Barkana, and M. Kamionkowski, *Phys. Rev. D* **98**, 103529 (2018), [arXiv:1807.11482 \[astro-ph.CO\]](#).
- [38] H. Liu, N. J. Outmezguine, D. Redigolo, and T. Volansky, *Phys. Rev. D* **100**, 123011 (2019), [arXiv:1908.06986 \[hep-ph\]](#).
- [39] H. Gies, J. Jaeckel, and A. Ringwald, *EPL* **76**, 794 (2006), [arXiv:hep-ph/0608238](#).
- [40] A. Berlin and A. Hook, *Phys. Rev. D* **102**, 035010 (2020), [arXiv:2001.02679 \[hep-ph\]](#).
- [41] A. Romanenko *et al.*, *Phys. Rev. Lett.* **130**, 261801 (2023), [arXiv:2301.11512 \[hep-ex\]](#).
- [42] A. Badertscher, P. Crivelli, W. Fetscher, U. Gendotti, S. Gninenko, V. Postoev, A. Rubbia, V. Samoylenko, and D. Sillou, *Phys. Rev. D* **75**, 032004 (2007), [arXiv:hep-ex/0609059](#).
- [43] M. Gluck, S. Rakshit, and E. Reya, *Phys. Rev. D* **76**, 091701 (2007), [arXiv:hep-ph/0703140](#).
- [44] H. Gies, J. Jaeckel, and A. Ringwald, *Phys. Rev. Lett.* **97**, 140402 (2006), [arXiv:hep-ph/0607118](#).
- [45] M. Ahlers, H. Gies, J. Jaeckel, J. Redondo, and A. Ringwald, *Phys. Rev. D* **77**, 095001 (2008), [arXiv:0711.4991 \[hep-ph\]](#).
- [46] F. Della Valle, E. Milotti, A. Ejlli, G. Messineo, L. Piemontese, G. Zavattini, U. Gastaldi, R. Pengo, and G. Ruoso, *Phys. Rev. D* **90**, 092003 (2014), [arXiv:1406.6518 \[quant-ph\]](#).
- [47] F. Della Valle, A. Ejlli, U. Gastaldi, G. Messineo, E. Milotti, R. Pengo, G. Ruoso, and G. Zavattini, *Eur. Phys. J. C* **76**, 24 (2016), [arXiv:1510.08052 \[physics.optics\]](#).
- [48] J. Jaeckel, *Phys. Rev. Lett.* **103**, 080402 (2009), [arXiv:0904.1547 \[hep-ph\]](#).
- [49] A. Caputo, L. Sberna, M. Frias, D. Blas, P. Pani, L. Shao, and W. Yan, *Phys. Rev. D* **100**, 063515 (2019), [arXiv:1902.02695 \[astro-ph.CO\]](#).
- [50] A. Berlin, R. T. D’Agnolo, S. A. R. Ellis, P. Schuster, and N. Toro, *Phys. Rev. Lett.* **124**, 011801 (2020), [arXiv:1908.06982 \[hep-ph\]](#).
- [51] A. Berlin and K. Schutz, *Phys. Rev. D* **105**, 095012 (2022), [arXiv:2111.01796 \[hep-ph\]](#).
- [52] A. Berlin, R. Tito D’Agnolo, S. A. R. Ellis, and J. I. Radkovski, *JHEP* **08**, 017 (2023), [arXiv:2305.05684 \[hep-ph\]](#).
- [53] R. N. Mohapatra and I. Z. Rothstein, *Phys. Lett. B* **247**, 593 (1990).
- [54] J. H. Chang, R. Essig, and S. D. McDermott, *JHEP* **09**, 051 (2018), [arXiv:1803.00993 \[hep-ph\]](#).
- [55] J. Bernstein, M. Ruderman, and G. Feinberg, *Phys. Rev.* **132**, 1227 (1963).
- [56] M. I. Dobroliubov and A. Y. Ignatiev, *Phys. Rev. Lett.* **65**, 679 (1990).
- [57] S. Davidson, B. Campbell, and D. C. Bailey, *Phys. Rev. D* **43**, 2314 (1991).
- [58] S. Davidson, S. Hannestad, and G. Raffelt, *JHEP* **05**, 003 (2000), [arXiv:hep-ph/0001179](#).
- [59] H. Vogel and J. Redondo, *JCAP* **02**, 029 (2014), [arXiv:1311.2600 \[hep-ph\]](#).
- [60] A. Stebbins and G. Krnjaic, *JCAP* **12**, 003 (2019), [arXiv:1908.05275 \[astro-ph.CO\]](#).
- [61] A. Melchiorri, A. Polosa, and A. Strumia, *Phys. Lett. B* **650**, 416 (2007), [arXiv:hep-ph/0703144](#).
- [62] Z. Bogorad and N. Toro, *JHEP* **07**, 035 (2022), [arXiv:2112.11476 \[hep-ph\]](#).
- [63] J. Jaeckel and A. Ringwald, *Ann. Rev. Nucl. Part. Sci.* **60**, 405 (2010), [arXiv:1002.0329 \[hep-ph\]](#).
- [64] M. A. Fedderke, P. W. Graham, D. F. J. Kimball, and S. Kalia, *Phys. Rev. D* **104**, 075023 (2021), [arXiv:2106.00022 \[hep-ph\]](#).
- [65] M. A. Fedderke, P. W. Graham, D. F. Jackson Kimball, and S. Kalia, *Phys. Rev. D* **104**, 095032 (2021), [arXiv:2108.08852 \[hep-ph\]](#).
- [66] A. Arza, M. A. Fedderke, P. W. Graham, D. F. J. Kimball, and S. Kalia, *Phys. Rev. D* **105**, 095007 (2022), [arXiv:2112.09620 \[hep-ph\]](#).
- [67] I. A. Sulai *et al.*, *Phys. Rev. D* **108**, 096026 (2023), [arXiv:2306.11575 \[hep-ph\]](#).
- [68] P. Sikivie, N. Sullivan, and D. B. Tanner, *Phys. Rev. Lett.* **112**, 131301 (2014), [arXiv:1310.8545 \[hep-ph\]](#).
- [69] L. Brouwer *et al.* (DMRadio), *Phys. Rev. D* **106**, 103008 (2022), [arXiv:2204.13781 \[hep-ex\]](#).
- [70] P. Arias, A. Arza, B. Döbrich, J. Gamboa, and F. Méndez, *Eur. Phys. J. C* **75**, 310 (2015), [arXiv:1411.4986 \[hep-ph\]](#).
- [71] P. Alken, E. Thébault, C. D. Beggan, H. Amit, J. Aubert, J. Baerenzung, T. Bondar, W. Brown, S. Califf, A. Chambodut, *et al.*, *Earth, Planets and Space* **73**, 1 (2021).
- [72] G. A. Glatzmaier and P. H. Roberts, *Physics of the Earth and Planetary Interiors* **91**, 63 (1995).
- [73] G. A. Glatzmaiers and P. H. Roberts, *Nature* **377**, 203 (1995).
- [74] C. Burrage, J. Jaeckel, J. Redondo, and A. Ringwald, *JCAP* **11**, 002 (2009), [arXiv:0909.0649 \[astro-ph.CO\]](#).
- [75] S. Davidson and M. E. Peskin, *Phys. Rev. D* **49**, 2114 (1994), [arXiv:hep-ph/9310288](#).
- [76] A. Berlin, R. Harnik, Y.-Y. Li, and B. Xu, (2024), [arXiv:2404.16094 \[hep-ph\]](#).
- [77] C. G. Constable and S. C. Constable, “Satellite magnetic field measurements: Applications in studying the deep earth,” in *The State of the Planet: Frontiers and Challenges in Geophysics* (American Geophysical Union,

- AGU, 2004) pp. 147–159.
- [78] G. Bevilacqua, V. Biancalana, P. Chessa, and Y. Dancheva, *Appl. Phys. B* **122**, 103 (2016), [arXiv:1601.06938 \[physics.ins-det\]](#).
- [79] G. Oelsner, R. IJsselsteijn, T. Scholtes, A. Krüger, V. Schultze, G. Seyffert, G. Werner, M. Jäger, A. Chwala, and R. Stolz, *Phys. Rev. Applied* **17**, 024034 (2022), [arXiv:2008.01570 \[physics.atom-ph\]](#).
- [80] G. Chatzidrosos, A. Wickenbrock, L. Bougas, N. Leefer, T. Wu, K. Jensen, Y. Dumeige, and D. Budker, *Phys. Rev. Applied* **8**, 044019 (2017), [arXiv:1706.02201 \[quant-ph\]](#).
- [81] A. T. Younesi, M. Omar, A. Wickenbrock, D. Budker, and R. Ulbricht, (2024), [arXiv:2410.20876 \[quant-ph\]](#).
- [82] B. A. Buffett, in *AGU Fall Meeting Abstracts*, Vol. 2011 (2011) pp. GP23B–01.
- [83] S. I. Braginsky and P. H. Roberts, *Geophysical and Astrophysical Fluid Dynamics* **79**, 1 (1995).
- [84] N. Gillet, D. Jault, E. Canet, and A. Fournier, *Nature* **465**, 74 (2010).
- [85] M. Landeau, A. Fournier, H.-C. Nataf, D. Cébron, and N. Schaeffer, *Nature Reviews Earth and Environment* **3**, 255 (2022).
- [86] C. G. Provatidis, *Physica Scripta* **99**, 025006 (2024).

## Supplemental Material: Geomagnetic Signal of Millicharged Dark Matter

Ariel Arza,<sup>1</sup> Yuanlin Gong,<sup>1,2</sup> Jing Shu,<sup>3,4,5</sup> Lei Wu,<sup>1</sup> Qiang Yuan,<sup>2,6</sup> Bin Zhu<sup>7</sup>

<sup>1</sup>*Department of Physics and Institute of Theoretical Physics, Nanjing Normal University, Nanjing, 210023, China*

<sup>2</sup>*Key Laboratory of Dark Matter and Space Astronomy, Purple Mountain Observatory, Chinese Academy of Sciences, Nanjing 210023, China*

<sup>3</sup>*School of Physics and State Key Laboratory of Nuclear Physics and Technology, Peking University, Beijing 100871, China*

<sup>4</sup>*Center for High Energy Physics, Peking University, Beijing 100871, China*

<sup>5</sup>*Beijing Laser Acceleration Innovation Center, Huairou, Beijing, 101400, China*

<sup>6</sup>*School of Astronomy and Space Science, University of Science and Technology of China, Hefei 230026, China*

<sup>7</sup>*School of Physics, Yantai University, Yantai 264005, China*

### FORMAL SOLUTION FOR THE VECTOR POTENTIAL

In this section, we show explicitly how to extract the vector potential for a given magnetic field model. The vector potential  $\vec{\mathcal{A}}$  can be found by solving  $\vec{\nabla} \times \vec{\mathcal{A}} = \vec{\mathcal{B}}$ . We write  $\vec{\mathcal{B}}$  and  $\vec{\mathcal{A}}$  in a vector spherical harmonics (VSH) expansion as

$$\vec{\mathcal{B}}(\vec{x}) = \sum_{\ell,m} \left( \mathcal{B}_r(r) \vec{Y}_{\ell m}(\theta, \varphi) + \mathcal{B}_1(r) \vec{\Psi}_{\ell m}(\theta, \varphi) + \mathcal{B}_2(r) \vec{\Phi}_{\ell m}(\theta, \varphi) \right), \quad (\text{S.1})$$

$$\vec{\mathcal{A}}(\vec{x}) = \sum_{\ell,m} \left( \mathcal{A}_r(r) \vec{Y}_{\ell m}(\theta, \varphi) + \mathcal{A}_1(r) \vec{\Psi}_{\ell m}(\theta, \varphi) + \mathcal{A}_2(r) \vec{\Phi}_{\ell m}(\theta, \varphi) \right), \quad (\text{S.2})$$

Where the  $\mathcal{B}_i$  and  $\mathcal{A}_i$  coefficients are also functions of  $\ell$  and  $m$ . The curl of the background vector potential is given by

$$\vec{\nabla} \times \vec{\mathcal{A}} = \sum_{\ell,m} \left( -\frac{\ell(\ell+1)}{r} \mathcal{A}_2 \vec{Y}_{\ell m} - \left( \frac{d\mathcal{A}_2}{dr} + \frac{\mathcal{A}_2}{r} \right) \vec{\Psi}_{\ell m} + \left( -\frac{\mathcal{A}_r}{r} + \frac{d\mathcal{A}_1}{dr} + \frac{\mathcal{A}_1}{r} \right) \vec{\Phi}_{\ell m} \right). \quad (\text{S.3})$$

By comparison we find the following set of first order ordinary equations for the components of the vector potential

$$\begin{aligned} -\frac{\ell(\ell+1)}{r} \mathcal{A}_2 &= \mathcal{B}_r, \\ \frac{d\mathcal{A}_2}{dr} + \frac{\mathcal{A}_2}{r} &= \mathcal{B}_1, \\ \frac{d\mathcal{A}_1}{dr} + \frac{\mathcal{A}_1}{r} - \frac{\mathcal{A}_r}{r} &= \mathcal{B}_2, \\ \frac{d\mathcal{A}_r}{dr} + \frac{2\mathcal{A}_r}{r} - \ell(\ell+1) \frac{\mathcal{A}_1}{r} &= 0. \end{aligned} \quad (\text{S.4})$$

where the last line is the gauge constraint  $\vec{\nabla} \cdot \vec{\mathcal{A}} = 0$ . From the first line of the Eq. (S.4) we extract

$$\mathcal{A}_2 = -\frac{r}{\ell(\ell+1)} \mathcal{B}_r, \quad (\text{S.5})$$

and the second line is just a redundancy of this (from  $\nabla \cdot \vec{\mathcal{B}} = 0$ ).  $\mathcal{A}_1$  and  $\mathcal{A}_r$  can be figured out by solving the system composed by the last two lines in Eqs. (S.4). We decouple this system finding a second order equation for  $\mathcal{A}_1$  given by

$$\frac{(r^2(r\mathcal{A}_1)')'}{r^3} - \frac{\ell(\ell+1)}{r^2} \mathcal{A}_1 = \frac{1}{r^3} (r^3 \mathcal{B}_2)'. \quad (\text{S.6})$$

A formal solution for the above equation is found through

$$\mathcal{A}_1 = \int dr' G_\ell(r, r') \frac{1}{r'^2} \frac{d}{dr'} (r'^3 \mathcal{B}_2(r')), \quad (\text{S.7})$$

where  $G_\ell(r, r')$  is the Green's function given by

$$G_\ell(r, r') = -\frac{1}{2\ell + 1} \begin{cases} (r/r')^{\ell-1}, & r < r' \\ (r'/r)^{\ell+2}, & r > r' \end{cases}. \quad (\text{S.8})$$

Once we get  $\mathcal{A}_1$  explicitly,  $\mathcal{A}_r$  is directly found by

$$\mathcal{A}_r = r \frac{d\mathcal{A}_1}{dr} + \mathcal{A}_1 - r\mathcal{B}_2. \quad (\text{S.9})$$

## MODEL FOR THE GEOMAGNETIC FIELD AND VECTOR POTENTIAL PROFILE

For clarity and later convenience, we note that there are three main regions for the structure of the Earth interior; the mantle, the outer core, and the inner core. These regions are separated by the Core-Mantle Boundary (CMB) and the Inner-Core Boundary (ICB), located at  $R_{\text{cmb}} = 3486$  km and  $R_{\text{icb}} = 1216$  km from the Earth center, respectively. The usual term ‘the core of the earth’ refers to the combination of the inner core and outer core. We take the radius of the Earth as  $R_e = 6371.2$  km.

We are interested in the profile of  $\vec{\mathcal{A}}$  for  $r \geq R_e$ . From Eq. (S.5) we get that the component  $\mathcal{A}_2$  is determined directly from  $\mathcal{B}_r$ . For this we can make use of the conventional IGRF model for the Earth's geomagnetic field, which is valid for  $r \geq R_{\text{cmb}}$  and can be written as

$$\vec{\mathcal{B}}(\vec{x}) = \sum_{\ell, m} C_{\ell m} \left( \frac{R_e}{r} \right)^{\ell+2} \left( (\ell + 1) \vec{Y}_{\ell m}(\theta, \varphi) - \vec{\Psi}_{\ell m}(\theta, \varphi) \right), \quad R_{\text{cmb}} \leq r, \quad (\text{S.10})$$

where the  $C_{\ell m}$  are coefficients given, for instance, in reference [71]. The spherical coordinates  $(r, \theta, \varphi)$  are attached at the Earth center with  $\theta$  and  $\varphi$  being the latitude, and longitude, respectively. We have

$$\mathcal{A}_2 = - \sum_{\ell, m} \frac{C_{\ell m}}{\ell} \frac{R_e^{\ell+2}}{r^{\ell+1}}, \quad R_{\text{cmb}} \leq r. \quad (\text{S.11})$$

As seen from Eq. (S.7) and Eq. (S.9), to get the profiles for the components  $\mathcal{A}_1$  and  $\mathcal{A}_r$ , we need a model for the magnetic field component  $\mathcal{B}_2$  for all values of  $r$ . It is clear from the IGRF model (Eq. (S.10)) that this component is absent for  $r \geq R_{\text{cmb}}$ . In fact, as will shown later, it only exists in the outer core, for  $R_{\text{icb}} \leq r \leq R_{\text{cmb}}$ . Unfortunately, there is no precise model for the  $\mathcal{B}_2$  profile. However, so far it is possible to infer a rms value of the total magnetic field over the outer core volume  $V_d$ , defined as

$$\mathcal{B}^{\text{rms}} = \sqrt{\frac{1}{V_d} \int [\vec{\mathcal{B}}(r, \theta, \varphi)]^2 dV}, \quad (\text{S.12})$$

where the integration in the radial coordinate is performed in the range  $R_{\text{icb}} \leq r \leq R_{\text{cmb}}$ . As pointed out in Refs. [82–85], the real value of  $\mathcal{B}^{\text{rms}}$  ranges from 2.5 to 10 mT. As we only have values for the total rms magnetic field, we need to have an idea of the other components, namely,  $\mathcal{B}_r$  and  $\mathcal{B}_1$ , to deduce the profile of  $\mathcal{B}_2$ .

To construct our model for the magnetic field in the core we use the fact that it is produced by electric currents  $\vec{J}$  that are only present in the outer core, i.e., for  $R_{\text{icb}} \leq r \leq R_{\text{cmb}}$ . Thus, we assume the following constraints:

- 1). the electric current merely lies in the outer core and is responsible for generating the full geomagnetic field inside and outside the Earth. The profile of the current is continuous and smooth.
- 2). the inner core has a constant magnetic field with magnitude  $\mathcal{B}_{\text{ic}} = 6$  mT [86].
- 3). the outer core has a rms magnetic field value between 2.5 mT and 10 mT.
- 4). the profile for the magnetic field is continuous and smooth.

To find the magnetic field sourced by electric currents  $\vec{J}$  in the outer core, we need to solve the system composed

by the equations  $\vec{\nabla} \times \vec{\mathcal{B}} = \vec{J}$  and  $\vec{\nabla} \cdot \vec{\mathcal{B}} = 0$ . As for  $\vec{\mathcal{B}}$  and  $\vec{\mathcal{A}}$ , we also write  $\vec{J}$  in a VSH expansion as

$$\vec{J}(\vec{x}) = \sum_{\ell, m} \left( J_r(r) \vec{Y}_{\ell m}(\theta, \varphi) + J_1(r) \vec{\Psi}_{\ell m}(\theta, \varphi) + J_2(r) \vec{\Phi}_{\ell m}(\theta, \varphi) \right). \quad (\text{S.13})$$

Due to the similarities of this system to the equations used to find the vector potential, we write the same solutions

$$\mathcal{B}_2 = -\frac{r}{\ell(\ell+1)} J_r, \quad (\text{S.14})$$

$$\mathcal{B}_1 = \int dr' G_\ell(r, r') \frac{1}{r'^3} \frac{d}{dr'} (r'^3 J_2(r')), \quad (\text{S.15})$$

$$\mathcal{B}_r = r \frac{d\mathcal{B}_1}{dr} + \mathcal{B}_1 - r J_2. \quad (\text{S.16})$$

From now, for convenience, we use the defined quantities  $x = \frac{r}{R_e}$ ,  $\vec{b} = \frac{\vec{\mathcal{B}}}{B_0}$  and  $\vec{j} = \frac{R_e \vec{J}}{B_0}$ , where  $B_0 = 2.94 \times 10^{-2}$  mT and is related to the coefficient  $C_{10}$  in Eq. (S.10) by  $C_{10} = -\sqrt{4\pi/3} B_0$ .  $B_0$  can also be interpreted as the value of the geomagnetic field at the equator of the Earth surface in a simple dipole model. As the uncertainty in the values of  $\mathcal{B}^{\text{rms}}$  is around 60%, we only consider the coefficients  $\ell = 1$  in all VSH expansions since higher orders contribute with corrections of only about 10% (at least for the IGRF model). We model the current density as the polynomial expansions

$$j_2 = (a_0 + a_1 x + a_2 x^2 + a_3 x^3 + a_4 x^4 + a_5 x^5) \delta_{m0}, \quad (\text{S.17})$$

$$j_r = -2\tilde{\beta} (x - x_{\text{icb}})^4 (x_{\text{cmb}} - x)^3 \delta_{m0}. \quad (\text{S.18})$$

From  $\vec{\nabla} \cdot \vec{j} = 0$  it is found that  $j_1 = j_r + x j'_r / 2$ . The coefficients  $a_i$  are found after imposing the boundary conditions

$$\begin{aligned} j_2(x_{\text{icb}}) &= 0, & j_2(x_{\text{cmb}}) &= 0, \\ j'_2(x_{\text{icb}}) &= 0, & j'_2(x_{\text{cmb}}) &= 0, \\ b_1(x_{\text{icb}}) &= \frac{1}{\sqrt{2}} \frac{\mathcal{B}_{\text{ic}}}{C_{10}}, & b_1(x_{\text{cmb}}) &= \sqrt{\frac{4\pi}{3}} \frac{1}{x_{\text{cmb}}^3}, \end{aligned} \quad (\text{S.19})$$

where  $b_1$  is calculated through Eq. (S.15). The profile of  $j_r$  satisfies a vanishing value for  $j_r$ ,  $j_1$  and their derivatives at the outer core boundaries. The  $(x - x_{\text{icb}})^4$  of the  $j_r$  profile makes the current density tends to be more prominent at locations closer to the boundary with the mantle. Finally, we use Eq. (S.12) to calculate  $\tilde{\beta}$ , assuming the value for  $\mathcal{B}^{\text{rms}}$  ranges between 2.5 and 10 mT. We get  $\tilde{\beta} = 1.2 \times 10^8 \beta$ , where  $\beta$  is a value ranging from 1 to 4.6, that accounts for the uncertainty in  $\mathcal{B}^{\text{rms}}$ . The profiles for the three components of the magnetic fields in the Earth interior are plotted in Fig. S1.

Using Eq. (S.7) and Eq. (S.9) and integrating by parts, we write the final expression for the vector potential as

$$\vec{\mathcal{A}} = -B_0 R_e \left( 1.01 \beta \left( \frac{R_e}{r} \right)^3 (2\vec{Y}_{10} - \vec{\Psi}_{10}) - \sqrt{\frac{4\pi}{3}} \left( \frac{R_e}{r} \right)^2 \vec{\Phi}_{10} \right), \quad R_e < r. \quad (\text{S.20})$$

As a final note, in Fig. S2, we show the illustration for the subdominant signal from the tangential effective current  $\vec{J}_{\text{eff}} = J_{\text{eff,t}} \vec{\Phi}_{10}$  that is proportional to the second term in Eq. (S.20). From the Ampere's law  $\oint d\vec{l} \cdot \vec{B} = \int d\vec{S} \cdot \vec{J}_{\text{eff}}$ , the Ampere loop showed in the Fig. S2 gives us  $2\pi R_e B \approx 2\pi R_e h J_{\text{eff,t}}$  and thus  $B \approx R_e (h/R_e) J_{\text{eff,t}}$  suppressed by the height of the ionosphere  $h \ll R_e$ . While the radial effective current  $\vec{J}_{\text{eff}} = J_{\text{eff,r}} \vec{Y}_{10}$  give us  $2\pi R_e B \approx \pi R_e^2 J_{\text{eff,r}}$  and thus is dominant signal of the form  $B \approx R_e J_{\text{eff,r}} / 2$  as shown in the Fig. 1 of the main text.

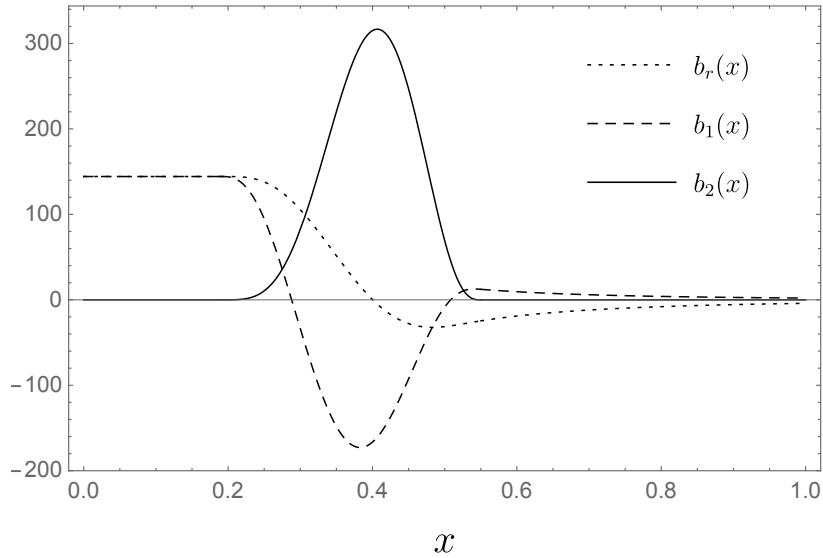


Figure S1. The profiles for  $b_r(x)$ ,  $b_1(x)$ , and  $b_2(x)$  of the magnetic fields in the Earth interior, with  $x = r/R_e$ .

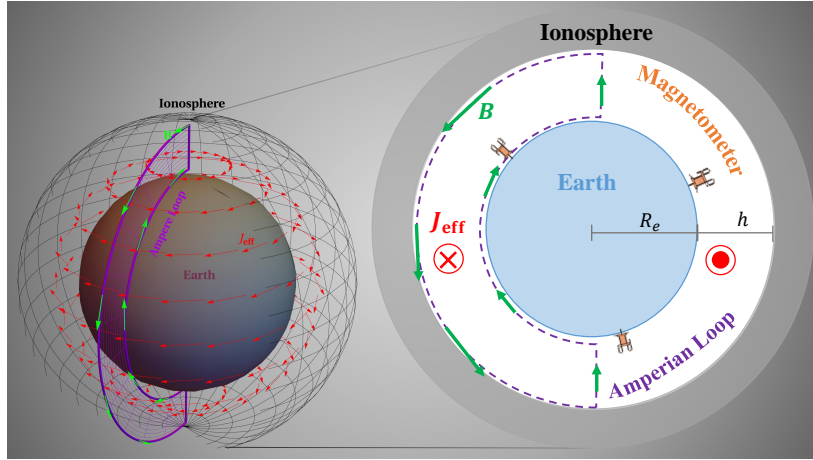


Figure S2. **Right:** Natural Earth's cavity formed between the Earth's surface and the ionosphere. It shows the tangential component of the dark matter effective current  $\vec{J}_{\text{eff}}$  passing through a chosen Amperian Loop. The generated magnetic field  $\vec{B}$  can be probed by the magnetometers (orange symbols) placed over the surface of the Earth. This shows schematically how for tangential components the generated magnetic field signal is suppressed by the ionosphere height  $h$ . **Left:** 3D version of the Right.

### CONSTRAINT FROM PHOTON TIME DELAY OF PULSARS

We start from the Lagrangian describing the millicharged dark matter (mDM)  $\phi$  coupling with photons  $A_\mu$

$$\mathcal{L} = (\partial_\mu \phi)^2 - \frac{1}{2} m_\phi^2 \phi^2 - i e_m A^\mu \phi^* \partial_\mu \phi - i e_m A^\mu \phi \partial_\mu \phi^* - e_m^2 \phi^2 A_\mu A^\mu - \frac{1}{4} F_{\mu\nu} F^{\mu\nu}, \quad (\text{S.21})$$

with  $e_m$  the millicharge,  $m_\phi$  the mass of mDM and  $F_{\mu\nu} = \partial_\mu A_\nu - \partial_\nu A_\mu$  is the electromagnetic field tensor. The E.o.M. of photons follows as,

$$\square^2 A_\mu + e_m^2 \phi^2 A_\mu = e_m J_{\text{eff}}^\mu, \quad (\text{S.22})$$

where  $J_{\text{eff}}^\mu = i(\phi^* \partial_\mu \phi - \phi \partial_\mu \phi^*) \sim 2e_m A^\mu |\phi|^2$  is the effective current. Note that the dark matter is typically assumed to be charge neutral thus contribute nothing to photons. To evaluate the response of mDM to a passing-by photon,

one can estimate  $e_m A^\mu$ , which results in a plasma mass  $m_{\text{pl}}$  from the mDM approximated as,

$$eJ_{\text{eff}}^\mu \approx 2e_m^2 \phi^2 A^\mu \approx m_{\text{pl}}^2 A^\mu. \quad (\text{S.23})$$

By assuming  $m_\phi$  is much smaller than the photon frequency  $\omega$ , one can Fourier transform Eq.(S.22) and use WKB approximation to neglect the oscillation of the mDM, arriving at,

$$(-\omega^2 + k^2 + e_m^2 \phi^2) A^\mu = 0. \quad (\text{S.24})$$

While the dispersion relation of photons is then modified as,

$$\omega^2 = k^2 + e_m^2 \langle \phi^2 \rangle \approx k^2 + 2e_m^2 \rho / m_\phi^2, \quad (\text{S.25})$$

where the  $\rho$  is the energy density of the mDM. The group velocity dispersion can be calculated as:

$$v_g = \frac{d\omega}{dk} = \frac{k}{\omega} \approx 1 - \frac{e_m^2 \rho}{m_\phi^2 \omega^2}. \quad (\text{S.26})$$

This will give rise to the change in the time of arrival (TOA) of a photon in the background of the mDM halo. Specifically, the TOA difference of a photon of  $\omega$  relative to photon with ultra high energy  $v_g = 1$  from a distant pulsar can be estimated as,

$$\Delta t_{\text{eff}}(\omega) = \int \frac{dl}{v_g} - dl \approx \frac{e_m^2}{m_\phi^2} (\omega^{-2}) \int \rho dl \equiv \frac{e^2}{m_e} (\omega^{-2}) \text{DM}_{\text{eff}}, \quad (\text{S.27})$$

where we introduce  $\text{DM}_{\text{eff}} \equiv \frac{e_m^2 m_e}{e^2 m_\phi^2} \int \rho dl$  as the effective dispersion measure. Here,  $e$ ,  $m_e$  is the electron charge and mass. In the standard model, time delay could be induced by the galactic electrons. Similarly, we can write down the TOA difference from galactic electrons with number density  $n_e$

$$\Delta t_e(\omega) \approx \frac{e^2}{m_e \omega^2} \int n_e dl \equiv \frac{e^2}{m_e} (\omega^{-2}) \text{DM}_e, \quad (\text{S.28})$$

where the dispersion measure  $\text{DM}_e$  for the electron is defined.

We have values for  $\text{DM}_e$  in astronomy for observed pulsars, roughly  $\text{DM}_e \sim 20 \text{ pc/cm}^3$  at a distance of  $d \sim 400 \text{ pc}$ . Thus we can conservatively constrain millicharge dark matter by requiring  $\text{DM}_{\text{eff}} \leq \text{DM}_e$ . With the approximation

$$\text{DM}_{\text{eff}} \equiv \frac{e_m^2 m_e}{e^2 m_\phi^2} \int \rho dl \approx \frac{e_m^2 m_e}{e^2 m_\phi^2} \rho d, \quad (\text{S.29})$$

we find the constraint on the  $e_m$  as

$$e_m \leq 6.61 \times 10^{-23} \times \left( \frac{m_\phi}{10^{-14} \text{ eV}} \right) \times \left( \frac{\text{DM}_e}{20 \text{ pc/cm}^3} \right)^{\frac{1}{2}} \times \left( \frac{0.3 \text{ GeV/cm}^3}{\rho} \right)^{\frac{1}{2}} \times \left( \frac{400 \text{ pc}}{d} \right). \quad (\text{S.30})$$